Monolayer Doping via Phosphonic Acid Grafting on Silicon: Microscopic Insight from Infrared Spectroscopy and Density Functional Theory Calculations

*Roberto C. Longo, Kyeongjae Cho, Wolf Gero Schmidt, Yves J. Chabal, and Peter Thissen**

Monolayer doping (MLD) is a promising technique for creating ultra shallow junctions (USJs). Here, a novel self assembled monolayer (SAM) grafting technique is proposed through a single oxygen atom capable of MLD. Consequently, this approach can use simple forms of alkylphosphonic acids and avoid carbon contamination altogether during the doping process. In this paper, density functional theory (DFT) is used to explore the way how alkylphosphonic acid molecules can in just one chemical step be grafted on H-terminated Si(111). A maximum coverage of alkylphosphonic acids is found at 2/3 due to steric constrain forces. It is further demonstrated by means of in situ infrared spectroscopy and DFT calculations that the weak link of an alkylphosphonic acid, such as octadecylphosphonic acid (ODPA), is the P-C bond, with typical release of the carbon ligand around 500 °C. Finally, after release of the carbon ligand, an unsaturated electron configuration is driving force for the phosphorous to start the MLD process.

1. Introduction

Density scaling and subsequent device dimension reduction continue to drive significant advances in the materials, processing, and architectural design of advanced transistors. As gate lengths approach the sub-10-nm regime, junction doping has become an increasing concern due to its importance in controlling short channel effects. Source/drain junction depths (or more specifically S/D extensions) must be extremely shallow and abrupt, typically around 1/3 of gate length (L_g). Unfortunately, the conventional technique for junction doping, ion implantation and anneal, is incapable of producing uniform and abrupt junctions below 10 nm in depth due to random dopant fluctuations and ion-induced damage leading to broadened dopant profiles. These concerns become magnified as the industry moves to Tri-gate (or similar) architectures where uniform, abrupt, non-damaged ultra shallow junctions (USJs) in a tight 3-dimensional pitch array is a necessity.

The technique of monolayer doping (MLD) is conceptually very attractive and has yielded encouraging initial results.[1,2] The MLD technique uses the self-limiting nature of self-assembled monolayers (SAMs) to produce a uniform coverage of a specific quantity of dopant containing molecules. In this approach, the coverage of the SAMs determines the areal dopant dose. Subsequent high temperature anneals drive the dopant atoms into the semiconductor via diffusion. Thermal treatment temperature and time govern the junction depth. Careful control of these parameters can provide a wide range of dopant profiles. Due to the control and uniformity of SAM attachment, precise dopant profiles less than 5 nm deep with an abruptness of sub 1 cm^{-3}/nm have been demonstrated with low sheet resistance.[1] Additionally, SAM attachment can easily be attained on multiple surface orientations on non-planar structures making MLD an ideal technique for uniform shallow doping of all three sides of a tri-gate device.[3]

Pioneering work in MLD has made use of dopant containing molecules with an alkene terminus for direct attachment to H-terminated Si through a standard hydrosilylation process. This requirement has limited the choice to allylboronic acid pinacol ester (for B) and diethyl 1-propylphosphonate (for P), and required the deposition of a relatively thick oxide overlayer to trap the dopant during annealing.[1,2] Consequently, the key road-block to further MLD development has been the control of the overall process to achieve reliable doping levels at predetermined depth without deleterious impurity incorporation since the dopant in these molecules is captured within a carbon network. Furthermore, the lack of in situ and spectroscopic characterization has prevented proper optimization of the annealing step.

In this paper, we combine in situ infrared spectroscopy and ab initio density functional theory (DFT) calculations to investigate a fundamentally different grafting method, based on a recent discovery[4–6] that makes it possible to directly attach the dopant on H-terminated Si through a single oxygen atom.[7] The process is based on the ability to graft alcohols directly to Si-H with a well controlled coverage (1/3 monolayer), and has now been extended to acids. In both cases, the relevant atom X is

Dr. R. C. Longo, Prof. K. Cho, Prof. Y. J. Chabal, Dr. P. Thissen
Department of Materials Science and Engineering
University of Texas at Dallas
800 West Campbell Road, Richardson, TX 75080, USA
E-mail: peter.thissen@utdallas.edu
Prof. W. G. Schmidt
Lehrstuhl für Theoretische Physik
Universität Paderborn
33098 Paderborn, Germany

DOI: 10.1002/adfm.201202808

attached to Si by forming a Si-O-X bond, where X can be P, As and other dopants. In this approach, simple forms of the acids (e.g., monohydride phosphonate) can be used to avoid carbon contamination altogether. Nonetheless, we demonstrate in force constant studies that the weak link of an alkylphosphonic acid, such as octadecylphosphonic acid (ODPA), is the X-C bond (P-C bond in this case), with typical release of the carbon ligand at 500 °C. Therefore, even if a long alkyl chain is preferred to better control the SAM formation, there is no need to protect the organic layer by an oxide layer, since the dopant remains at the surface at a temperature where all carbon ligands (potential C contaminants) are removed. Furthermore, the hydrogen from neighboring Si-H unit desorbs below 500 °C, opening a path for dopant diffusion. An unsaturated electron configuration after the release of the carbon chain is a rather strong driving force to start that process.

2. Results and Discussion

Figure 1 (bottom line) shows all of the typical spectral features of a monodentate phosphonic acid:[11,26–28] the stretch mode of the (P = O) at 1227 cm^{-1}, the asymmetric and symmetric stretch modes of the (P–O) at 1078 and 1004 cm^{-1}, and the deformation mode of the (P–O–H) feature clearly present at 956 cm^{-1}.[29] In the aliphatic region, the spectral positions of the strong asymmetric and symmetric stretch modes of the (CH_2) at 2918 and 2850 cm^{-1}, respectively, indicate an ordered arrangement on the surface. In addition, the asymmetric and symmetric stretch modes of the (CH_3) at 2966 and 2870 cm^{-1} are present. The temperature of the sample was increased stepwise from RT to 700 °C. In-situ taken IR measurements are shown in Figure 1. Heating steps to 300 °C do not show any change in the system. Between 400 and 500 °C one can see a clear removal of the carbon chain, but no remove of the phosphonic acid anchor group. This means, that the ODPA molecules break at the P-C connection. The P–C bond breakage is essential and has to be substantiated. We first integrate the area of the CH_x modes between 3000 cm^{-1} and 2800 cm^{-1} at room temperature to use as a reference corresponding to 1 ML. After annealing to 700 °C, the remaining amount of hydrocarbons is found to be ~23% of the starting amount (i.e. ~0.23 ML). It is believed that the remaining amount comes from the poor vacuum conditions leading to some re-adsorption after the anneal because it is not consistent with LEIS data performed in UHV. An ultra-high vacuum system for the IR measurements would therefore be necessary to confirm this point. Further experiments to substantiate the point of the P–C breakage and the SAMs uniformity were performed by XPS and AFM. Their results are shown in the supplementary information. A further increasing of the temperature leads to oxidation of the sample (Figure 1), which can be recognized from the peaks at 1180 cm^{-1} $(S–O)^{LO}$ and 1030 cm^{-1} $(S–O)^{TO}$. These peaks shift to higher wavenumbers when the SiO_2 is growing.

In an interesting experiment, Torun et al. removed an ODPA SAM from an Al_2O_3(0001) surface using the AFM.[30] Although the experiment was performed in a solvent, re-adsorption was not observed. This might be a hint that not the whole molecule but only the carbon chain has been removed.

In order to develop an accurate picture of the adsorption process described in the previous paragraph, we performed DFT and DFT-D simulations. First, we will describe the grafting method of methylphosphonic acid (MPA) on H-terminated Si(111) surface and discuss the kinetics of the chemical reaction:

$$Si - H + CH_3OP(OH)_2 \rightarrow Si - OCH_3OPOH + H_2 \quad (1)$$

Next, we describe in detail the grafting process of the MPA to the Si(111) surface taking the nanopattern configuration as an example. To calculate the kinetic barrier of the adsorption pathway one has to follow the system from the initial situation where one of the molecules is over the surface to the final configuration. This reaction pathway is illustrated in **Figure 2**, where we show the variation of the energy profile as a function

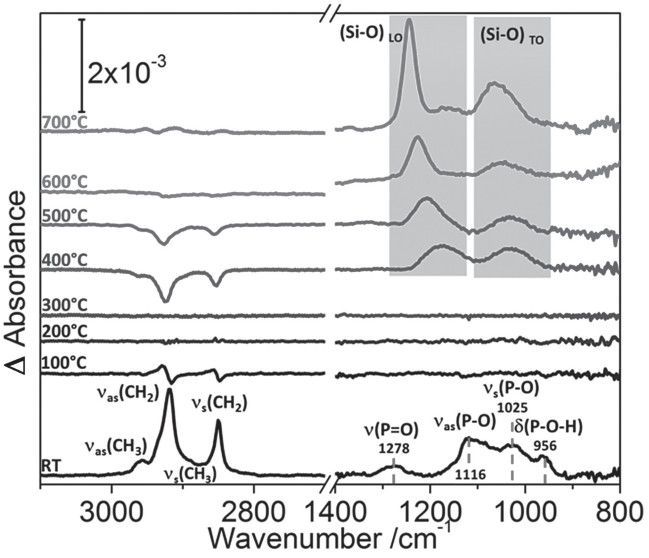

Figure 1. Differential infrared absorption spectra: Transmission spectra taken after heating adsorbed ODPA on oxide-free silicon surface at different temperatures; each spectrum is referenced to the one measured before.

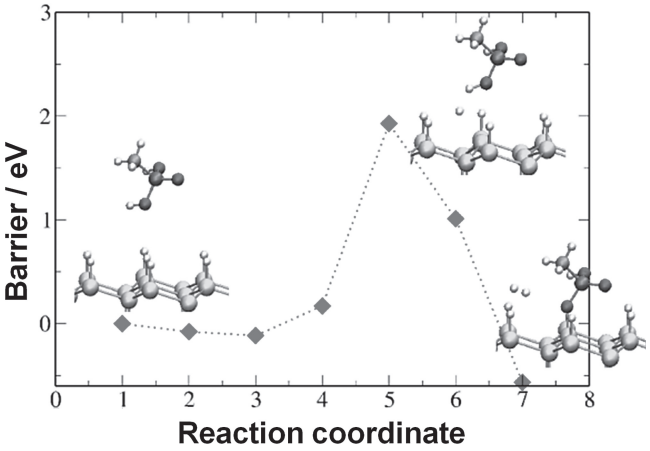

Figure 2. Kinetic barrier for the grafting process of the MPA on the Si(111) surface. The insets show the initial, transition and final states, respectively. Yellow spheres represent Si atoms; white, H; red, O; blue, C and brown spheres P atoms, respectively.

of the distance between images used in the construction of the elastic band of the NEB method. The pictures in the inset show the initial, transition-state (TS), and final configurations, respectively. Several considerations are in order. First, as the molecule approaches the Si(111) surface, it undergoes physisorption without any kinetic barrier. The energy gain for this process is 0.11 eV and the lowest distance between oxygen and Si atoms is 3.87 Å. Second, the barrier for the chemical grafting of the phosphonic acid to the Si(111) surface is relatively high, 2.03 eV. The reason for this is twofold: the higher surface energy of the Si(111) surface compared to more-open surfaces like Si(100), and the high coverage of our Si(111) model system, which is fully H-terminated and with the other two molecules of the nanopattern already grafted to the surface. The TS shows that the surface loses its hydrogen before the phosphonic acid molecule. Alternative reaction paths with the molecule loosing the H atom first or both atoms of the H_2 molecule (the reaction product) at the same time show even higher barriers.

Our calculations indicate that the monodentate configuration is the only chemisorption geometry possible for MPA adsorption on this oxide-free H-terminated Si(111) surface. The energy associated with bi- and tri-dentate is substantially higher due to large strains needed to link three H centers separated by 3.9 Å to the oxygen atoms of the phosphonic acid head separated by 2.3 Å.[31]

This reaction pathway profits from the flexibility of the silicon atoms in top position of the silicon lattice. This can reduce the kinetic barriers due to concerted chemical reactions by ~1 eV. These processes are known in the literature for long time as lattice assisted processes. They can be enhanced if the temperature is increased and thereby the silicon phonons are excited. These effects are commonly not observed on metal surfaces or play only a minor role there. They are a consequence of the localized nature of the covalent bonds of silicon and therefore probably of general importance for the understanding of semiconductor surfaces.

Next, the ubiquitous questions of maximum coverage, molecule-surface, molecule-molecule interactions and resulting structures are discussed in detail.

Starting from the lowest energy adsorption configuration of a single MPA unit on the H-terminated Si(111) surface unit cell, the MPA coverage was systematically increased to six MPA units, corresponding to a 2/3 monolayer. The corresponding lowest energy structures obtained from various starting geometries for the respective coverage on the surface are shown in **Figure 3**.

Here and in the following, the notation MPA_n^l refers to structures with n MPA units per unit cell and l describing the configuration of the molecular interaction. The adsorption energy E_{ads} as a function of the number of MPA units adsorbed on the H-terminated Si(111) surface following the chemical reaction showed in Equation 1 has been calculated with respect to the MPA molecule in vacuum and the clean H-terminated Si(111) surface slab

$$E_{ads} = \frac{E_n - E_o - n * E_{MPA} + E_{H_2}}{n} \quad (2)$$

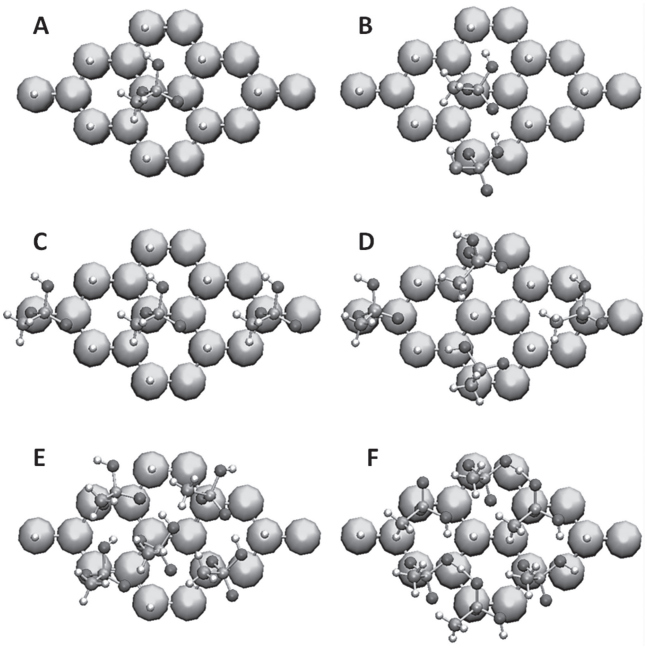

Figure 3. Relevant energy structures obtained for different coverages of the MPA_n (n = 1–6) on the Si(111) surface. Yellow spheres represent Si atoms, white, H; red, O; blue, C and pink spheres P atoms, respectively. In correlation with Figure 5 the configurations are B-NN; C-nanopattern; D-island; E-five and F-ring.

Additionally, the H-bond strength was calculated for every MPA configuration, following an universal relationship between the H-bond length and strength from Jones et al.[32] Finally, the strain energy was calculated following the approach suggested by Nemanick et al.[33] All results are summarized in **Figure 4**.

We find the adsorption energy and the H-bond strength to be specially low at dimers. These structures seem to be

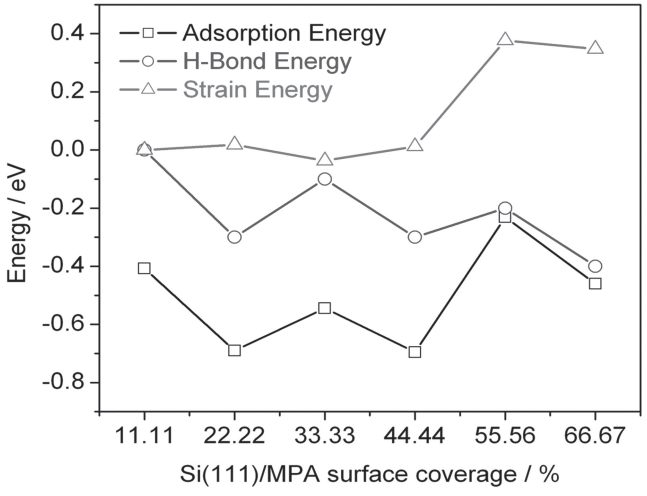

Figure 4. Adsorption, H-bond and strain energies of the MPA on the Si (111) surface as a function of the coverage. The values presented are calculated always for the lowest energy configuration.

energetically favorized on the Si(111) surface. Furthermore, the strain energy does not allow any higher coverage than 2/3.

However, the adsorption energy alone does not allow to conclude on the stability of a specific surface structure. Rather, one has to take into account the chemical potentials $\mu(A_i)$ of the surface constituents A_i in order to energetically compare interfaces with different stoichiometries. The ground state of the surface is determined by the minimum of the thermodynamic grandcanonical potential Ω,

$$\Omega = F - \sum_i \mu(A_i) * n_{A_i} \quad (3)$$

where $F = E–TS$ is the surface free energy which we approximate by the total surface energy E at zero temperature assuming similar entropy contributions S for different adsorption configurations. In fact, the differences in vibrational free energy and electronic entropy are typically several orders of magnitude smaller than the adsorption energies calculated here. If one assumes a flat, stoichiometric, H-terminated Si(111) surface in the presence of MPA, the grandcanonical potential will mainly depend on the chemical potential of MPA. **Figure 5** shows the resulting phase diagram. Interestingly, we note that again the dimer structures are energetically favorized.

Next we consider alkyl chain phosphonic acid molecules to confirm the understanding of the structure and interaction of the monodentates. We have studied the oxygen-oxygen distance (P=O to P–O–H of the neighboring phosphonic acid molecule) as a function of the alkyl chain lengths. As the alkyl chain length increases, the distance between the two oxygen increases (**Table 1**). The reason is an additional gain of enthalpy from van der Waals forces with longer alkyl chains. The van der Waals forces dictate the position of the chains and thereby a certain tilt to optimize the chains interaction. Tilting the alkyl chain directly influences the position of P=O and P–O–H and thereby the distance.

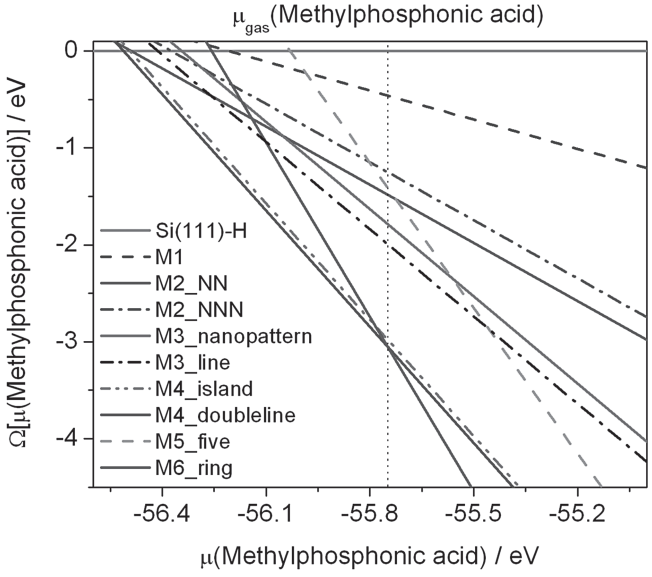

Figure 5. Grand canonical potential of the different structures considered in this work as a function of the MPA_n (n = 1–6) chemical potential. In correlation with figure 3 the configurations are B-NN; C-nanopattern; D-island; E-five and F-ring.

Table 1. Tilt angles and Si-O, P-O, average CH_2 and O-O (see text) bond lengths for the nanopattern coverage as a function of the number of carbon atoms of the alkyl chain, obtained with both PBE-GGA and DFT-D (in parenthesis) functionals.

N	Tilt Angle [Degrees]	Si-O [Å]	P-O [Å]	C-H2 [Å]	O-O [Å]
1	80.00 (81.45)	1.69 (1.69)	1.47 (1.47)	1.09 (1.09)	
2	79.12 (82.23)	1.69 (1.70)	1.47 (1.47)	1.09 (1.09)	4.18 (4.25)
3	78.73 (84.51)	1.69 (1.70)	1.47 (1.47)	1.09 (1.09)	4.19 (4.29)
4	89.41 (90.92)	1.70 (1.70)	1.47 (1.47)	1.09 (1.09)	4.26 (4.27)
5	87.77 (88.33)	1.70 (1.70)	1.47 (1.47)	1.09 (1.10)	4.27 (4.27)
6	87.82 (90.37)	1.70 (1.70)	1.47 (1.47)	1.09 (1.10)	4.27 (4.32)
7	86.37 (87.05)	1.70 (1.70)	1.47 (1.47)	1.10 (1.10)	4.29 (4.33)
8	90.46 (91.22)	1.71 (1.70)	1.48 (1.47)	1.10 (1.10)	4.30 (4.33)

Table 1 also shows the tilt angles and the Si–O, P–O and CH_2 bond lengths obtained at 0 K, within both PBE-GGA and DFT-D schemes. These bond lengths do not appreciably change with the functional used in the calculations. The results appear to be remarkably different if we look into the vibrational properties. Indeed, although the phosphonic acid-alkyl chains are all very stable structures, specially the nanopattern configuration, the inter-molecular CH_2 and O–O interactions, which to a large extent determine the main features of the IR spectra, cannot be fully described within the standard PBE-GGA theory. The relaxation process is mainly driven by the intra-molecular forces and the surface-phosphonic acid interactions, which are much more stronger in magnitude than the van der Waals forces. These forces lead the whole system to its minimum energy configuration.

Nevertheless, the vibrational properties are obtained as the second derivative of the energy with respect to the position of the atoms, i.e., a small change in the position of the atoms in the molecule can strongly affect its vibrational motion and hence the frequency we measure in the IR spectra. This effect is well noted in the calculated vibrational frequencies of the CH_2 groups of the alkyl chains. If we do not include the van der Waals forces in our simulations, the amplitude of the vibrational motion of the CH_2 groups is not affected by the neighboring molecules and, as a consequence, the vibrational frequencies are higher. Taking into account the van der Waals forces, the frequencies are reduced by 20 cm^{-1}, approximately (see **Figure 6**).

Our calculations also show that the coupling between the vibrational modes of the CH_2 groups inside the molecules are very strong, specially for the longer alkyl chains and for the CH_2 groups closer to the head of the molecule (CH_3). If this degree of freedom is not included in the calculations, all the modes are shifted by an average of 50 cm^{-1}. It has been widely shown that the antisymmetric modes always carry more energy, because their vibrational motion is less affected by the presence of the neighboring CH_2, specially in well-ordered systems like alkylphosphonic acids chains supported on the Si(111) surface.

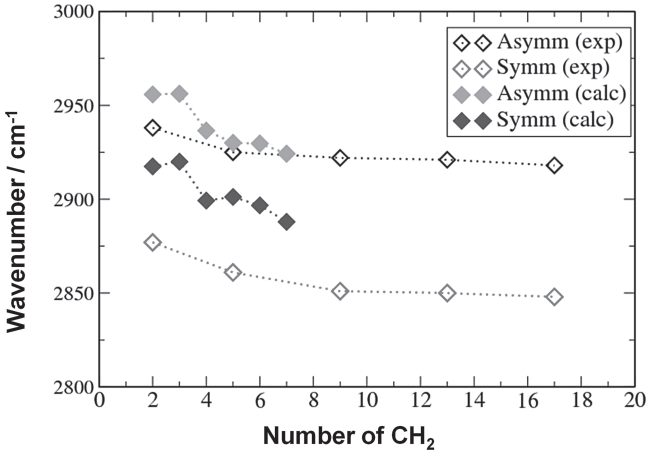

Figure 6. Experimental and calculated (DFT-D) vibrational spectra of the symmetric and asymmetric modes of the alkylphosphonic acid molecules (nanopattern configuration) on the Si(111) surface as a function of the number of CH_2 groups of the alkylphosphonic acid molecules.

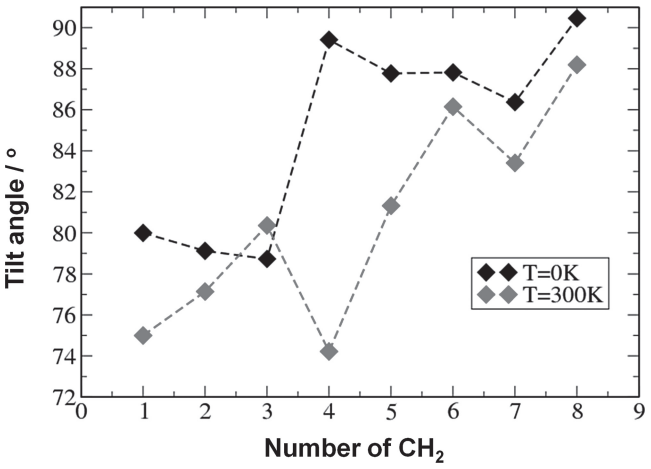

Figure 7. Calculated tilt angle at 0 and 300 K of the MPA (nanopattern configuration) on the Si(111) surface as a function of the number of CH_2 groups of the MPA molecules.

Our DFT obtained frequencies follow the same trend as the experimental ones, and the shift induced by the van der Waals interactions improves the agreement with the experimentally obtained results, specially for the modes that carry more energy (asymmetric).

In order to gain more insight into the molecular interactions, we have studied the molecular tilt angle of the phosphonic acids adsorbed in nanopattern configuration and how the tilt changes with the length of the alkyl chain. It has already been shown that a change in molecular tilt can experimentally be obtained by comparing the s- and p-polarized IR spectra.[34] We calculated the tilt angle of the chains as the angle between the top C atom of the chain and a line connecting two Si atoms of the top layer of the Si(111) surface. To obtain the change in the tilt as a function of temperature, we performed ab initio molecular dynamics (MD) simulations. Starting from the relaxed geometries at O K, we gradually increased the temperature of the system by re-scaling the velocities every 10 steps, performing at each step a fully relaxation of the system using the velocity Verlet algorithm.[35] The time step used in our simulations is 0.5 fs and the final temperature is 300 K. At 0 K, the tilt angle is close to the normal with respect to the surface, as one should expect because it corresponds to the most stable configuration of the nanopattern. The longer the alkyl chain, the bigger the tilt angle obtained is (closer to 90º). If we increase the temperature (see **Figures 7** and **8**), we can see two different regions: if the length of the chain is higher than 4 (number of CH_2), the van der Waals interactions of the head groups of the chain (CH_3) predominate over the H-bond interactions. For alkyl chains lower than 4 CH_2 groups, the H-bond interactions predominate over the van der Waals inter-molecular interactions.

Finally, we have performed stress tests on adsorbed MPA to determine the weak link in molecules described in the first paragraph of this section.

Starting from the relaxed structure, we froze the Si-bulk and build up a force-field on the CH_3-group of the alkylphosphonic acids to release them from the surface. To describe in detail the desorption process of the alkylphosphonic acid from the Si(111) surface, taking the nanopattern coverage as an example, we have calculated the kinetic barrier for the desorption pathway followed by the system from the initial situation to the final configuration. This reaction pathway is illustrated in Figure 8, where we show the variation of the energy profile as a function of the distance between images used in the construction of the elastic band of the NEB method. The main results from these calculations are: (1) The weak link of alkylphosphonic acids, such as ODPA, is the P-C bond and (2) after release of the carbon chain, the phosphorous remains with a dangling bond. The fastest way to satisfy the unsaturated electron configuration is a relaxation of the structure and thereby starting the monolayer doping process. Full research of the diffusion pathway during the ML process is beyond the scope of this work.

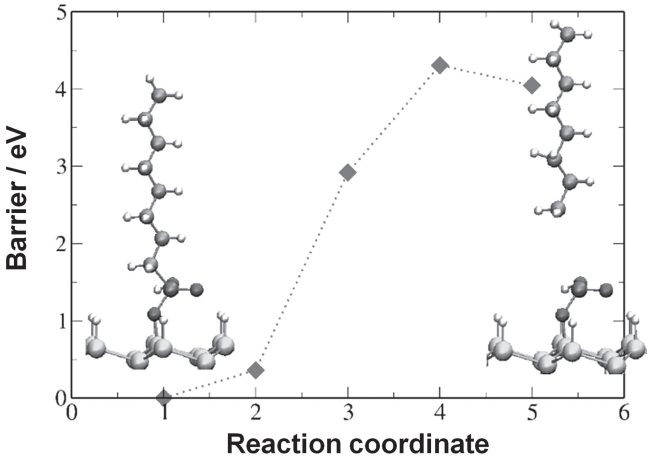

Figure 8. Kinetic barrier to desorb the top group of the octylphosphonic acid (OPA) on the Si(111) surface. The insets show the initial and final states, respectively. Yellow spheres represent Si atoms, white, H; red, O; blue, C and brown spheres P atoms, respectively.

3. Conclusions

First, we have described the grafting method of phosphonic acids on H-terminated silicon(111) and discussed the kinetics of the chemical reaction. Experimentally, we have established, that in a solution of phosphonic acid with alcohols as solvent the acid and not the alcohol is grafted.

Second, the ubiquitous questions of maximum coverage, molecule-surface, molecule-molecule interactions and resulting structures were discussed in detail. We find the adsorption energy and the H-bond strength to be specially deep at dimers. These structures seem to be energetically favorized on the Si(111) surface. Furthermore, the strain energy does not allow any higher coverage than 2/3.

Finally, we have performed stress tests on adsorbed alkylphosphonic acids and determined the weak link in molecules with typical release temperatures. The weak link of alkylphosphonic acids is the P-C bond and this weak link is released typically around 500 °C. After release of the carbon chain, the phosphorous remains with a dangling bond. The fastest way to satisfy the unsaturated electron configuration is a relaxation of the structure and thereby starting the monolayer doping process.

Our DFT calculated results were confirmed in an in-situ infrared study. We adsorbed ODPA on an H-terminated oxide-free silicon(111) sample and heated it up under vacuum conditions. Around 500 °C, the carbon chain was released while the phosphonic anchor stayed at the surface.

4. Experimental Methods and Computational Details

Sample Preparation: A 3.8 cm × 1.5 cm wafer of Float Zone (FZ) Si(111) double side polished is cleaned in piranha solution (H_2SO_4 (Fisher 98%):H_2O_2 (Fisher 30%) 3:1) for 30 min, intensely rinsed with deionized H_2O (18.2 MΩ cm Mili Q), and finally dried in a stream of N_2. Samples were H-terminated by a 30 s dip in 10% HF(aq) followed by a 2.5 min dip in 40% NH_4F(aq), and a final rinse in H_2O for 30 s. This produces an atomically smooth (111)-oriented Si surface for tens to hundreds of nanometers. Afterward the sample is coated with ODPA by immersion into a 10–3 mol methanol solution at 65 °C for 12h (in a glovebox). The environment control is critical to avoid oxidation of the surface.[8–10] In Situ Surface Analysis: The surface analysis is performed in a Quartz chamber capable of working in continuous vacuum (p = 10–4 Torr) or under the flow of different gas phase molecules. Samples can also be resistively heated to 1000 °C.[11] An infrared (IR) spectrometer (Thermo Scientific, Nicolet 6700) allows in situ analysis of the sample during the execution of the process. IR measurements are performed with a deuterated triglycine sulfate (DTGS) detector with 3000 averaged scans to ensure an optimal signal-to-noise ratio. Computational Details: The calculations were performed using DFT within the generalized gradient approximation (GGA) as implemented in the Vienna ab initio simulation package (VASP).[12–16] The electron-ion interaction was described within the projector-augmented wave (PAW) scheme. The electronic wave functions were expanded into plane waves up to a kinetic energy of 360 eV. The surface was modeled by periodically repeated slabs. The supercell used here consisted of 8 atomic layers of Si plus adsorbed molecules and a vacuum region equivalent to 16 atomic layers. The 7 uppermost layers of Si as well as the adsorbate degrees of freedom were allowed to relax until the forces on the atoms are below 10 meV/Å. The Brillouin zone integration was performed using 4 × 4 × 1 mesh within the Monkhorst-Pack scheme.[17] The PBE functional was used to describe the electron exchange and correlation energy within the GGA.[18] Eigenmodes were calculated by the force-constant (FC) approach, diagonalizing the mass weighted second derivative matrix (Hessian) in case of the adsorbed species and the top Si layer.[19,20] The restriction to the atoms of the top layer and the adsorbed species is legitimate because the Eigenmodes of these atoms do not overlap with the Eigenmodes of the bulk material. Kinetic barriers were calculated by the nudged elastic band (NEB) method,[21] using a string of geometric configurations to describe the reaction pathway of the system. A spring interaction between every configuration ensured continuity of the reaction pathway. Although density functionals that account for nonlocal vdW interactions have been developed, see, for example, ref. [22,23], the numerical cost restricts their application to relatively simple systems. A pragmatic, numerically far less demanding way to treat dispersion forces is been given by the DFT-D approach,[24,25] where the vdW forces are obtained as a sum over pair-wise, parametrized interactions. In the following study we use the DFT-D parameters suggested by Grimme.[24]

Supporting Information

Supporting Information is available from the Wiley Online Library or from the author.

Acknowledgements

C. Hinkle is acknowledged for very fruitful discussions. A. Vega is acknowledged for experimental support. P.T. and W.G.S. acknowledge the DFG for financial support. The authors acknowledge the Texas Advanced Computing Center (TACC) for computational resources.

Received: September 26, 2012
Revised: December 17, 2012
Published online: February 18, 2013

[1] K. W. Ang, J. Barnett, W. Y. Loh, J. Huang, B. G. Min, P. Y. Hung, I. Ok, J. H. Yum, G. Bersuker, M. Rodgers, V. Kaushik, S. Gausepohl, C. Hobbs, P. D. Kirsch, R. Jammy, *IEEE Int. Electron Devices Meeting* **2011**.
[2] J. C. Ho, R. Yerushalmi, G. Smith, P. Majhi, J. Bennett, J. Halim, V. N. Faifer, A. Javey, *Nano Lett.* **2009**, *9*, 725–730.
[3] O. Seitz, L. Caillard, H. M. Nguyen, C. Chiles, Y. J. Chabal, A. V. Malko, *Appl. Phys Lett.* **2012**, *100*.
[4] D. J. Michalak, S. R. Amy, D. Aureau, M. Dai, A. Esteve, Y. J. Chabal, *Nat. Mater.* **2010**, *9*, 266–271.
[5] D. J. Michalak, S. R. Amy, A. Esteve, Y. J. Chabal, *J. Phys. Chem. C* **2008**, *112*, 11907–11919.
[6] D. J. Michalak, S. Rivillon, Y. J. Chabal, A. Esteve, N. S. Lewis, *J. Phys. Chem. B* **2006**, *110*, 20426–20434.
[7] P. Thissen, O. Seitz, Y. J. Chabal, *Prog. Surf. Sci.* **2012**, *87*, 272–290.
[8] G. S. Higashi, Y. J. Chabal, G. W. Trucks, K. Raghavachari, *Appl. Phys. Lett.* **1990**, *56*, 656–658.
[9] B. B. Stefanov, A. B. Gurevich, M. K. Weldon, K. Raghavachari, Y. J. Chabal, *Phys. Rev. Lett.* **1998**, *81*, 3908–3911.
[10] M. K. Weldon, B. B. Stefanov, K. Raghavachari, Y. J. Chabal, *Phys. Rev. Lett.* **1997**, *79*, 2851–2854.
[11] A. Vega, P. Thissen, Y. J. Chabal, *Langmuir* **2012**, *28*, 8046–8051.
[12] G. Kresse, J. Furthmuller, *ut. Mater. Sci.* **1996**, *6*, 15–50.
[13] G. Kresse, J. Furthmuller, *Phys. Rev. B* **1996**, *54*, 11169–11186.
[14] G. Kresse, D. Joubert, *Phys. Rev. B* **1999**, *59*, 1758–1775.
[15] J. P. Perdew, J. A. Chevary, S. H. Vosko, K. A. Jackson, M. R. Pederson, D. J. Singh, C. Fiolhais, *Phys. Rev. B* **1992**, *46*, 6671–6687.
[16] J. P. Perdew, J. A. Chevary, S. H. Vosko, K. A. Jackson, M. R. Pederson, D. J. Singh, C. Fiolhais, *Phys. Rev. B* **1993**, *48*, 4978–4978.

[17] H. J. Monkhorst, J. D. Pack, *Phys. Rev. B* **1976**, *13*, 5188–5192.
[18] J. P. Perdew, K. Burke, M. Ernzerhof, *Phys. Rev. Lett.* **1996**, *77*, 3865–3868.
[19] S. Baroni, P. Giannozzi, A. Testa, *Phys. Rev. Lett.* **1987**, *58*, 1861–1864.
[20] B. N. Harmon, W. Weber, D. R. Hamann, *J. Phys. (Paris)* **1981**, *42*, 628–630.
[21] H. Jonsson, G. Mills, K. W. Jacobsen, In *Classical and Quantum Dynamics in Condensed Phase Simulations* (Ed: B. J. Berne, G. Ciccotti, D. F. Coker), World Scientific, Singapore **1998.**
[22] M. Dion, H. Rydberg, E. Schroder, D. C. Langreth, B. I. Lundqvist, *Phys. Rev. Lett.* **2004**, *92*, 246401.
[23] M. Dion, H. Rydberg, E. Schroder, D. C. Langreth, B. I. Lundqvist, *Phys. Rev. Lett.* **2005**, *95*, 109902.
[24] S. Grimme *J. Comp. Chem.* **2006**, *27*, 1787–1799.
[25] F. Ortmann, F. Bechstedt, W. G. Schmidt, *Phys. Rev. B* **2006**, *73*.
[26] P. Thissen, T. Peixoto, R. C. Longo, W. Peng, W. G. Schmidt, K. Cho, Y. J. Chabal, *J. Am. Chem. Soc.* **2012**, *134*, 8869–8874.
[27] P. Thissen, M. Valtiner, G. Grundmeier, *Langmuir* **2010**, *26*, 156–164.
[28] P. Thissen, J. Wielant, M. Koeyer, S. Toews, G. Grundmeier, *Surf. Coat. Technol.* **2010**, *204*, 3578–3584.
[29] P. Thissen, A. Vega, T. Peixoto, Y. J. Chabal, *Langmuir* **2012**.
[30] B. Torun, B. Ozkaya, G. Grundmeier, *Langmuir* **2012**, *28*, 6919–6927.
[31] P. Thissen, T. Peixoto, R. C. Longo, W. Peng, W. G. Schmidt, K. Cho, Y. J. Chabal, *J. Am. Chem. Soc* **2012**, *134*, 8869–8874.
[32] G. Jones, S. J. Jenkins, D. A. King, *Surf. Sci.* **2006**, *600*, L224–L228.
[33] E. J. Nemanick, S. D. Solares, W. A. Goddard III, N. S. Lewis, *J. Phys. Chem. B* **2006**, *110*, 14842–14848.
[34] H. Shpaisman, O. Seitz, O. Yaffe, K. Roodenko, L. Scheres, H. Zuilhof, Y. J. Chabal, T. Sueyoshi, S. Kera, N. Ueno, A. Vilan, D. Cahen, *Chem. Sci.* **2012**, *3*, 851–862.
[35] M. P. Allen, D. J. Tildesley, *Computer Simulation of Liquids*, Oxford University Press, Oxford **1990**.